Hydrothermal synthesis of needle-like nanocrystalline zeolites from metakaolin and their applications for efficient removal of organic pollutants and heavy metals

Hongwei Luo[a,b], Wei Wee Law[c], Yichao Wu[c,d], Weiping Zhu[c], En-Hua Yang[c,*]

[a]College of Environment, Zhejiang University of Technology, Hangzhou, 310014, China

[b]Energy Research Institute, Nanyang Technological University, Singapore 637553

[c]School of Civil and Environmental Engineering, Nanyang Technological University, Singapore 639798

[d]State Key Laboratory of Agricultural Microbiology, College of Resources and Environment, Huazhong Agricultural University, Wuhan, 430070, China

Abstract

In this study, an environment-friendly and sustainable route to convert clay minerals into highly efficient sorbents for organic pollutants and heavy metals removal was reported. Needle-like nanocrystalline zeolites were hydrothermally synthesized from metakaolin (MK) and their properties and efficiency for organic pollutants and heavy metals removal were investigated. After hydrothermal treatment, the morphology of metakaolin markedly transformed from layered structures to aggregations of needle-like zeolites, thereby resulting in substantial increases of total and meso porosities, N_2 sorption capacity and specific surface area. The hydrothermally synthesized MK-based zeolites exhibited much stronger sorption capacity toward aniline (AN), 3-chloroaniline (3-CA), and humic acid (HA). The electrostatic attraction and surface complexation dominated by chemisorption likely accounted for the enhanced

* Corresponding author: Tel: +65 6790 5291; Fax: +65 6791 0676; Email: ehyang@ntu.edu.sg (E.H. Yang)

sorptive interactions between zeolites and organic compounds. Similarly, the adsorption capacity of the newly formed zeolites toward Cu(II) and Pb(II) increased almost 20-fold, which was 431.0 mg g^{-1} for Cu(II) and 337.8 mg g^{-1} for Pb(II). Ionic exchange reactions between heavy metal ions and the enriched sodium ion resulted in heavy metal removal by the MK-based zeolites. Thus, the hydrothermally synthesized MK-based zeolites may be employed as sorbents for wastewater treatment to remove organic pollutants and heavy metals with no significant toxicity risk.

***Keywords*:** Zeolites; hydrothermal treatment; metakaolin (MK); organic pollutants; heavy metals

1. Introduction

Zeolites are a large group of natural and synthetic hydrated aluminosilicate minerals commonly used as commercial adsorbents and catalysts [1]. The special crystal structures of zeolites consist of three-dimensional frameworks of $(SiO_4)^{4-}$ and $(AlO_4)^{5-}$ tetrahedra with variable pore size and morphology [2]. The net negative charge of lattice is compensated by the exchangeable cations such as Na^+, K^+ and Ca^{2+}. These exchangeable cations in zeolites are usually innocuous, making them particularly suitable for removing toxic heavy metal ions (Cu^{2+}, Pb^{2+}, Cd^{2+}, Mn^{2+}, Hg^{2+}, etc.) from industrial effluent [3]. In addition, the removal of organic pollutants (dyes, humic substances, phenolic compounds, pesticides, pharmaceuticals, etc.) by natural zeolites and their modified forms has been extensively investigated [4-8], although zeolites exhibit relatively weak affinity toward organic pollutants. The electrostatic attraction and surface complexation dominate the chemisorption. To keep up with the global

rapidly growing water demand, it is of great interest to develop low-cost and sustainable adsorbents for the removal of toxic heavy metals and organic pollutants from wastewater [9]. The applications of zeolites for water and wastewater treatment have been focused mainly due to their properties and significant worldwide occurrence. Currently, the use of zeolites is still a promising technique in environmental remediation processes [1]. Zeolites are preferably prepared from pure chemicals of sodium silicate and sodium aluminate. Nevertheless, their production from cheap natural clay minerals is of economic importance and therefore it is necessary to optimize the synthesis route [10].

Metakaolin ($Al_2O_3 \cdot 2SiO_2$), a calcined product of kaolin ($Al_2O_3 \cdot 2SiO_2 \cdot 2H_2O$) with Si/Al ratio of 1, is a very convenient raw material for the synthesis of zeolites due to its low cost and natural abundance. Several synthetic methods have been reported to use the natural raw materials (kaolin and metakaolin) for the production of zeolites. For example, zeolite A was previously synthesized from metakaolin using a microwave-assisted heating procedure [11,12]. However, hydrothermal method was a more popular way to produce zeolites and only few research work has been carried out using metakaolin as a starting material [3]. The removal of organic pollutants and heavy metals by the hydrothermally synthesized zeolites from raw metakaolin has not been well established and sufficiently documented. As a promising method, hydrothermal synthesis of zeolites is a multiphase reaction containing dissolution and crystallization process, which commonly involves at least one liquid phase and both amorphous and crystalline solid phases [13]. Thus, hydrothermal transformation of metakaolin into zeolites provides an alternative solution to sustainability of both clay mineral utilization and water contamination.

The main objective of this study is to explore the hydrothermal transformation of metakaolin into zeolites and their applications in efficient removal of organic pollutants and heavy metals. A layer-structured metakaolin was converted into needle-like nanocrystalline zeolites through hydrothermal treatment, thereby showing strongly enhanced sorption performance toward organic pollutants and heavy metals. The chemical, morphological and mineralogical properties of raw metakaolin and the converted zeolites were characterized. The specific surface area and pore size distribution were determined. The removal efficiencies of aniline (AN), 3-chloroaniline (3-CA), and humic acid (HA) were investigated using raw metakaolin and the hydrothermally synthesized MK-based zeolites. Their adsorption capacities toward Cu(II) and Pb(II) were further examined via sorption isotherms. Together, these experimental results are of environmental significance because they are useful to understand zeolites formation from metakaolin and subsequent removal of pollutants at contaminated sites.

2. Materials and methods

2.1. Hydrothermal treatment of metakaolin

Raw metakaolin (MK) samples were provided by BASF (Germany), and directly used without further treatment. The chemical compositions of the raw and the hydrothermally treated MK were determined using a sequential X-ray fluorescence (XRF) spectrometer (S8 Tiger, Bruker).

In previous publications, the synthesis of zeolite was carried out through two different routes: (1) conventional hydrothermal alkaline activation [14,15]; and (2) alkaline fusion prior to hydrothermal reaction [16]. In the first method, a calculated amount of NaOH pellets was

added to distilled water in reaction plastic beakers (150-250 ml) to prepare NaOH solutions, in which metakaolinite was added. In the second method, an alkaline fusion step was introduced prior to hydrothermal treatment. Metakaolinite was dry mixed with NaOH powder and the resultant mixture was fused at 600 °C for 1 h. The fused product was ground in a mortar and then a calculated amount of the ground powder was added to distilled water under stirring conditions. In both routes, chemical reagents, such as $CaCO_3$, $Al(OH)_3$, and precipitated SiO_2, were used as activators to control the Si/Al ratio.

In the current study, only raw metakaolin and NaOH were used as the starting materials, no additional Ca, Si and Al elements were introduced. Hydrothermal treatment of metakaolin was performed in slurry using a 45 mL Teflon-lined acid digestion bomb (Parr Instrument Company, USA). Initially, 5.0 g metakaolin powder was mixed with 30 mL of 2.0 M NaOH solution (liquid-to-solid ratio = 6) in a 50 mL plastic centrifuge tube and stirred for 30 min. The slurry was then transferred into the stainless steel autoclave, carefully sealed and incubated under 180 °C in the oven for 20 h. After hydrothermal reactions, the products were cooled to room temperature and subsequently washed three times by repeated centrifugation (5 min at 8000 g, 25 °C) using deionized water, and finally dried in oven at 105 °C for 6 h to recover the robust materials [15].

2.2. Characterization of raw and treated metakaolin

The morphology of the raw and the hydrothermally treated metakaolin was observed on a field emission scanning electron microscope (FESEM, JSM-7600F, JEOL). Before the test, the samples were treated by gold coating. Powder X-ray diffraction (XRD) patterns were taken on

a Bruker AXS D8 advance diffractometer using Cu Kα radiation (λ = 0.15406 nm). The tube voltage was 40 kV and the current was 40 mA. The XRD diffraction patterns were obtained in the 2θ range of 5-80° at a scan speed of 4° min^{-1}. Phase identification was carried out by searching the ICDD powder diffraction file database and comparing with those included in the Joint Committee on Powder Diffraction Standards (JCPDS) files [3,16]. Infrared (IR) spectra of metakaolin samples before and after hydrothermal treatment were recorded in the range of 480-4000 cm^{-1} on a Nicolet iS50 FT-IR spectrometer (Thermo Scientific, USA).

An automated surface area and pore size analyzer (Quadrasorb evo, Quantachrome Instruments) was employed to determine the specific surface area upon the Brunauer-Emmett-Teller (BET) nitrogen adsorption/desorption isotherms. Accordingly, the pore size distributions were calculated using the desorption Barrett-Joyner-Halenda (BJH) method. The outgas temperature and time were set at 180 °C and 18 hrs, respectively. Data analysis was performed using the QuadraWin software.

Thermogravimetric analysis (TGA) of the raw and converted materials was conducted with a TGA 8000 thermal analyzer (PerkinElmer, USA). Experiments were performed under a nitrogen atmosphere with a flow rate of 20 mL min^{-1} and at a heating rate of 10 °C min^{-1} from 30 °C to 900 °C.

2.3. Batch sorption experiments

Two heavy metals (Cu^{2+} and Pb^{2+}) and three organic pollutants (aniline (AN), 3-chloroaniline (3-CA), and humic acid (HA)) were chosen as models for sorption investigation. Pb(II) and Cu(II) ions were used in the form of $Pb(NO_3)_2$ and $Cu(NO_3)_2$, respectively. Aniline

and 3-chloroaniline were provided by Sigma-Aldrich, USA. Humic acid was purchased from International Humic Substances Society (IHSS).

The sorption kinetics were obtained by adding 0.1 g of metakaolin samples into 50 mL working solutions with either 400 mg L^{-1} organic pollutants or 1000 mg L^{-1} heavy metals. All assays were prepared in triplicate. The solution pH was adjusted to 3.0-5.0 for heavy metals and 7.2 for organic pollutants using 2 wt.% HNO_3 or NaOH. The mixture was stirred at 200 rpm and 25 °C. At specified time intervals, 1 mL of the mixture was taken and sacrificed to quantify the residual concentrations of each species e.g. Cu(II), Pb(II), AN, 3-CA, and HA. Samples were ten-times diluted and then filtered through 0.2-μm Acrodisc polyethersulfone membrane syringe filters (Pall Corp., Singapore) prior to analysis. The concentration of humic acid was characterized with total organic carbon and determined using TOC measurements (TOC-LCPH, Shimadzu Corp., Japan). The concentrations of AN and 3-CA in the aqueous solution were quantified using a reverse-phase high-performance liquid chromatography (HPLC, LC-20A, Shimadzu) equipped with a SIL-20A autosampler, LC-20AD solvent delivery system, and SPD-M20A photo-diode array (PDA) detector [17]. Operating conditions included an Acsentis C18 column (100 mm × 2.1 mm, 5 μm particle size), mobile phase of methanol-water (50/50 v/v), flow rate of 0.6 mL min^{-1} and detector set at 254 or 280 nm. The concentrations of Cu(II) and Pb(II) in the solution were measured by an inductively coupled plasma-mass spectrometer (ICP-MS, ELAN DRC-e, PerkinElmer).

To obtain the adsorption isotherm of MK toward Cu(II) and Pb(II), batch sorption experiments were conducted using 100 mL shaking flasks, in which 50 mL of Cu(II) or Pb(II) working solution and 0.1 g of metakaolin samples were added. Initial concentrations of heavy

metals were 50-2500 mg L^{-1} in the raw MK and 100-5000 mg L^{-1} in the treated MK, respectively. To prevent the precipitation, the solution pH was adjusted to 5.0 using 2 wt.% HNO_3. The reactants were mixed together and allowed to react at 25 °C for 18 h and equilibrate on an orbital shaker of 200 rpm (SKF-3100, Jeio Tech). After equilibration, the concentrations of remaining free heavy metal ions in the solution were measured to calculate the adsorption amount by MK.

The adsorption process of Cu(II) and Pb(II) from aqueous solution onto the raw and the treated MK was described by the Langmuir isotherm equation, which has been widely used in previous studies to explore the adsorption isotherms and to determine the maximum adsorption capacity of sorbent materials toward pollutants [8,17,18]. Following is a linearized form of the Langmuir isotherm:

$$\frac{C_e}{q_e} = \frac{C_e}{q_{\max}} + \frac{1}{bq_{\max}}$$

where C_e is the residual Cu(II) or Pb(II) concentration at equilibrium (mg L^{-1}); q_e is the amount of Cu(II) or Pb(II) adsorbed at equilibrium (mg g^{-1}); $q_{\max}$ is the maximum adsorption capacity of MK at equilibrium (mg g^{-1}); and b (L mg^{-1}) is the Langmuir constant [19,20].

3. Results and discussion

3.1. Chemical compositions revealed by XRF

Table 1 presents the XRF results of the raw and treated MK. As shown, the raw MK supplied by BASF Company was mainly composed of SiO_2 (53.01%) and Al_2O_3 (43.74%). After hydrothermal conversion, the treated MK consists of SiO_2 (41.32%), Al_2O_3 (34.36%), and Na_2O (21.79%). This observation suggested that NaOH solution was substantially

176 incorporated into the starting material, because except for 2 M of NaOH no other chemicals
177 were involved in the hydrothermal reactions of raw MK. In order to remove the excess NaOH,
178 the reaction products were washed by repeated centrifugation using deionized water until the
179 solution pH reached 7.2. Therefore, the XRF measurements indicated NaOH was chemically
180 incorporated into SiO_2 and Al_2O_3, leading to the decreased contents of Si and Al and the
181 increased content of Na.
182
183 *3.2. Morphology of raw and treated MK*
184 Fig. 1 shows the morphology of the raw (upper) and the hydrothermally treated (bottom)
185 MK at the similar magnifications. As can be seen, significant changes in morphology of MK
186 were observed following the hydrothermal treatment. The microstructure of raw MK particles
187 was platy in shape and had tendency to create higher agglomerate of circle shape. SEM
188 micrographs of the samples suggest that the surface was layered structure for raw MK. This
189 sheet-like form may be attributed to the dehydroxylation of kaolin, which was an endothermic
190 process due to the large amount of energy required to remove the chemically bonded hydroxyl
191 ions [21]. Above certain temperature range, kaolinite transforms into MK, a complex
192 amorphous structure which retains some long-range order due to layer stacking [22]. However,
193 the sheet-like MK was converted into needle-like nanocrystal materials after hydrothermal
194 treatment (Fig. 1). These remarkable changes in surface morphology and internal structure
195 were caused by the formation of new crystal phases under alkaline condition. More specifically,
196 the hydrothermal synthesis of needle-like nanomaterials was achieved through the alkali-
197 activated dissolution of Si and Al-containing minerals and subsequent re-precipitation with Na.

198 Thus, the reaction products may be mostly zeolite-type minerals [23,24]. To the best of our
199 knowledge, the current study is the first one to report and synthesize the needle-shaped zeolite
200 nanocrystals using a commercial MK sample as the starting material.
201
202 *3.3. Characterizations of MK by FTIR, XRD, and TGA*
203 Fig. 2a shows the FT-IR spectra of the raw and the hydrothermally treated MK. As can be
204 seen, similar patterns were observed at large wavenumber. For example, the broad band at
205 about 3400 cm^{-1} signified the O-H stretching vibrations of the H-O-H, Si-OH and Al-OH
206 groups. The spectral band at 1640 cm^{-1} in the treated MK was attributed to the zeolitic water
207 or the bending O-H bond of water molecules retained in the silica matrix [23]. In contrast, the
208 main difference of FT-IR spectra occurred in the lower absorption bands, especially between
209 550-1050 cm^{-1}. For the raw MK, the vibration bands located at 1050 cm^{-1} and 787 cm^{-1} were
210 assigned to the stretching Si-O bonds in SiO_2 and Al-O bonds in Al_2O_3, respectively [10,25].
211 After hydrothermal treatment, the band of 1050 cm^{-1} was shifted to that of 950 cm^{-1} and the
212 weak peak at 787 cm^{-1} disappeared. These changes were caused by antisymmetric stretching
213 of Si-O and Al-O bonds in aluminosilicates with zeolite or sodalite structure [10]. As known,
214 SiO_2 and Al_2O_3 were converted into aluminosilicates during the reactions between raw MK and
215 NaOH. Accordingly, their vibration bands were replaced by a strong single band around 950
216 cm^{-1}, characteristic of Si-O-Al bonds in TO_4 (T = Si or Al) tetrahedra in zeolite or
217 hydroxysodalite structure [25,26]. Moreover, three well-defined peaks at 550 cm^{-1}, 620 cm^{-1},
218 and 668 cm^{-1} were assigned to vibration of 4-membered and 6-membered rings from the
219 cancrinite ε-cage framework [27] or the symmetric T-O-T vibrations of sodalite framework.

This finding was in good agreement with that reported for hydroxysodalite zeolite [28]. In particular, the peak at 550 cm^{-1} indicated the presence of zeolite NaA band corresponding to the cubic prism [28].

Fig. 2b shows the XRD patterns of the raw and treated MK. As can be seen, the raw MK acquired from BASF Company was of amorphous structure and no distinct diffraction peaks could be observed. According to previous studies, the amorphous phase in the raw MK was relatively reactive in alkaline medium to produce either geopolymers [29] or zeolites [3]. Generally, the raw MK was a calcined and dehydroxylated product of the clay mineral kaolinite ($Al_2Si_2O_5(OH)_4$) [23]. Depending on the calcination temperature, the reactivity and property of raw MK could be quite different from each other. For example, to produce an amorphous and highly pozzolanic state of raw MK, nearly complete dehydroxylation was necessary under the appropriate temperature, because overheating caused sintering and thus formed a nonreactive refractory which contained mullite and a Si-Al defect spinel [21,22]. Therefore, the kaolin would be converted into an activated and metastable MK as expected when calcined between 600 °C and 850 °C, due to the structural disorder [30]. After hydrothermal treatment, the characteristic peaks in Fig. 2b became observable and the peak intensity markedly increased for the treated MK. Peak identification was further conducted using the Search-Match Software, and peak positions were compared with the database of powder diffraction file (PDF). The identified crystalline compounds were partially listed as follows: cancrisilite ($Na_7(Al_5Si_7O_{24})CO_3 \cdot 3H_2O$, PDF #00-046-1381), sodium aluminum silicate hydrate ($Na_3Al_3Si_3O_{12} \cdot 2H_2O$, PDF #00-044-0050), ZSM-22 (SiO_2, PDF #01-079-0564), and vishnevite ($Na_8Al_6Si_6O_{24}SO_4 \cdot 2H_2O$, PDF #00-046-1333). Additionally, the treated MK

products in Fig. 2b also matched the characteristic peaks of zeolite A/NaA and hydroxysodalite at 2θ values of 8.1°, 10.9°, 12.0°, 14.0°, 16.2°, 18.9°, 20.3°, 24.2°, 26.3°, 27.4°, 30.2°, 31.4°, 32.6°, 34.3°, 36.8°, 42.6° and 48.7° [23,31]. Coincided with the FT-IR results, the mineralogical analysis indicated that the needle-like zeolitic adsorbents were hydrothermally synthesized using raw MK powder as the starting material. The reaction mechanism includes the dissolution of MK under alkaline condition to release Si and Al, and subsequently re-precipitation, nucleation and crystallization of zeolites [16]. The entire process involves a heterogeneous nucleation mechanism and the presence of an aluminosilicate gel in the early stages [32]. The formation of different shapes such as needle and sheet is determined by the Si/Al ratio [33].

Fig. 2c shows the TGA curves of the raw and the treated MK. As can be seen, the raw MK exhibited a mass loss of less than 2%, whereas a mass loss of 14% was observed for the treated MK. It is known that the absorbed water in pores or on the surfaces was released at low temperature [10]. Thus, the accumulated loss between 100 °C and 175 ºC in the treated MK may be related to the loss of water located in the upper cages of the zeolite structure, while the loss at higher temperature could be attributed to the more tightly bound molecules in the sodalite cage [34]. The thermal behavior of the treated MK revealed a continuous weight loss up to ~600 ºC, which was attributed to the dehydration and decomposition processes, consistent with previous reports in which the thermal transition from cancrisilite to nepheline was complete at 600 °C [35].

3.4. BET surface area and porosity

Surface properties of the raw and the treated MK are illustrated in Fig. 3. The N_2 adsorption-desorption isotherms of the raw and treated MK are shown in Fig. 3a. After hydrothermal treatment, substantial increase in N_2 sorption capacity of MK was observed. Specifically, the calculated BET surface area of MK increased from 12.59 to 29.84 $m^2 g^{-1}$ (Fig. 3a), suggesting the evolution of porosity and potential for pollutants removal. As per the instructions from IUPAC, the N_2 sorption isotherms could be classified as type IV with a hysteresis loop of type H3 [36,37]. At high relative pressure, the presence of the hysteresis loop indicated a mesoporous structure in the treated MK, whereas the N_2 sorption capacity was attributed to the micropores at low relative pressure [17]. Fig. 3b shows the cumulative pore volume as a function of pore radius. As can be seen, the pore volume of the treated MK which was indicative of total porosity ($cm^3 g^{-1}$) increased much faster than that of the raw MK, especially at a larger pore radius. Fig. 3c further shows the differential pore size distribution, which was derived from the curve in Fig. 3b and obtained according to the Desorption Barrett-Joyner-Halenda (BJH) method. The pore size distribution confirmed the presence of the mesopores both in the raw and the treated MK with an average radius of 20.4±0.1 Å. The intensity of the sharp peak indicating the presence of mesopores remarkably increased following hydrothermal treatment. Therefore, the hydrothermal treatment significantly changed the porosity, the pore structure, and the adsorption capacity of MK likely due to the reactions and the newly formed zeolitic materials.

3.5. Time-dependent adsorption of organic pollutants

285 The kinetic behavior which controls the adsorption mechanism was studied to evaluate
286 the uptake rate of aniline (AN) and 3-chloroaniline (3-CA) from aqueous solution by MK. Fig.
287 4a shows the profiles of the sorption kinetics of AN and 3-CA by the raw and the treated MK.
288 As can be seen, the raw MK exhibited very limited sorption capacity toward AN and 3-CA,
289 which was 19.2±1.0 mg g^{-1} for AN and 18.5±0.1 mg g^{-1} for 3-CA. In contrast, the treated MK
290 showed a significantly enhanced sorption capacity toward AN and 3-CA, which was 143.0±3.7
291 mg g^{-1} for AN and 138.9±0.1 mg g^{-1} for 3-CA. These results are much higher than other
292 reported common sorbents such as clay minerals [38], incineration bottom ash [17], porous
293 carbons [39], modified biomass [40] and even zeolites [8], suggesting that MK materials,
294 especially after hydrothermal treatment, could be employed as the efficient sorbents for the
295 removal of organic pollutants from aqueous solution.
296 To further examine the proposed kinetic behavior of MK, humic acid (HA) was selected
297 as a model of organic pollutants. Fig. 4b shows the sorption kinetics of HA by the raw and the
298 treated MK. As can be seen, the sorption capacity of the treated MK increased by about 40%
299 compared to that of the raw MK, indicating the needle-like crystal structures of zeolites (Fig.
300 1) could result in a higher removal efficiency of organic pollutants than the sheet-like
301 amorphous structures of raw MK. The superior sorption performance of the treated MK toward
302 HA was attributed to the improved surface properties and also comparable to other sorbent
303 materials such as a modified zeolite [7], bentonite clay [41], and bottom ash [9]. As known,
304 zeolites are typically three dimensional aluminosilicate minerals that have valuable
305 physicochemical properties, such as cation exchange, molecular sieving, catalysis and
306 adsorption. They are promising due to their unique structures, uniform pores and channels, high

surface area and an excellent adsorption capacity for pollutants [1]. In current study, the electrostatic attraction and surface complexation dominated by chemisorption might account for the enhanced sorptive interactions between MK (zeolites) and organic compounds.

3.6. Sorption kinetics and isotherms of heavy metals

Fig. 5a shows the sorption kinetics of Cu(II) onto the raw and the treated MK at pH 3.0 and 5.0, in order to investigate the effects of pH on the adsorption process. It is known that the pH value of the aqueous solution is an important controlling parameter in the adsorption process because it can affect the surface charge of adsorbent, the degree of ionization and speciation of adsorbate during adsorption. According to previous studies, the adsorption capacity toward Cu(II) was very low at strong acidic medium (pH less than 2.0) and the adsorption capacity increases with increasing pH values, until a certain pH value was reached at 5.0. Accordingly, a sharp increase in the Cu(II) adsorption was observed when the pH increased from 3.0 to 5.0 [42]. Therefore, the pH of 3.0 and 5.0 are the critical values for investigation of Cu(II) adsorption. The effect of pH on Pb(II) adsorption is similar to Cu(II) ions [43] and only pH value of 5.0 has been chosen in the current study to obtain the maximum adsorption capacity. As can be seen, the treated MK obviously exhibited a much higher Cu(II) removal efficiency than the raw MK. Experiments carried out at pH 5.0 showed higher sorption and removal efficiency that that at pH 3.0. Similar reaction patterns were also observed for Pb(II) in Fig. 5b, where the treated MK was much more effective than the raw MK in removing Pb(II) ions. In general, the raw MK itself was not a good choice as the sorbent material for heavy metals removal, because very few exchangeable ions (Na^+, K^+ and Ca^{2+}) (shown in Table

1) were present in the amorphous sheet-like structures (Fig. 1). However, the hydrothermally treated MK was identified as zeolites (Fig. 2), which consisted of three-dimensional frameworks of SiO_4 and AlO_4 tetrahedra [2]. The Al^{3+} ion occupied the position in the center of the tetrahedron that was surrounded by four oxygen atoms, while the isomorphous replacement of Si^{4+} by Al^{3+} produced the negative charge in the lattice. The net negative charge was further balanced by the exchangeable cation such as Na^+ used in current study. Consequently, the Na^+ ion could be exchangeable with certain cations in aqueous solution such as Cu(II) (Fig. 5a) and Pb(II) (Fig. 5b). In fact, the exchangeable ions in zeolites were usually innocuous (sodium, potassium, and calcium ions), thereby making them particularly suitable for removing undesirable heavy metal ions from industrial effluent [1,2]. In addition, the adsorption capacity of Cu(II) increased as the solution pH increased from 3.0 to 5.0 (Fig. 5a). The lower Cu(II) uptake at pH 3.0 could be attributed to the increased competition for sorption sites with protons [44]. The concentration of protons at pH 3.0 was relatively high and the metal binding sites became positively charged repelling the Cu(II) uptake.

The Langmuir model was used to determine the maximum adsorption capacity of the raw and treated MK toward Cu(II) and Pb(II). Fig. 6 shows the adsorption data of Cu(II) and Pb(II), which were fitted well by a linearized form of Langmuir isotherm equation with the correlation factor of $R^2 > 0.98$, and thus other adsorption isotherms such as Freundlich were not considered in the current study. This finding suggested that the adsorption process was thermodynamically favorable and the adsorption of heavy metal ions onto the surface sites of sorbents could be modeled by monolayer adsorption [45]. Analysis of the data in Fig. 6 further revealed that the maximum adsorption capacity of the raw MK was 19.7±1.0 mg g^{-1} for Cu(II) (Fig. 6a) and

17.5±1.0 mg g^{-1} for Pb(II) (Fig. 6b). The Langmuir constant was calculated to be 0.011 and 0.111 L mg^{-1}, respectively. In contrast, the maximum adsorption capacity of the treated MK was 431.0±27.5 mg g^{-1} for Cu(II) (Fig. 6c) and 337.8±19.7 mg g^{-1} for Pb(II) (Fig. 6d) with the Langmuir constant of 0.009 and 0.047 L mg^{-1}, respectively. Compared to the raw MK, the adsorption capacity of the treated MK increased almost 20-fold, which was much higher than other sorbent materials such as natural zeolites [2], the MK-based geopolymer [46], and even the MK-based zeolites [3]. These experimental results indicated that the hydrothermally treated MK was a promising sorbent to efficiently remove the heavy metal ions like Cu(II) and Pb(II) from industrial wastewaters.

4. Conclusions

In this study, the needle-like nano-zeolites were hydrothermally synthesized using a raw metakaolin. Their potential applications in efficient removal of organic pollutants and heavy metals were further investigated. Results showed that the morphology of MK significantly changed from sheet-like layered structures to aggregation of needle-like zeolites after hydrothermal treatment, simultaneously resulting in substantial increases of total and meso porosities, N_2 sorption capacity and specific surface area. Compared to the raw MK, the hydrothermally treated MK exhibited a strongly enhanced sorption capacity toward aniline, 3-chloroaniline, and humic acid, which was even higher than other reported sorbents. The electrostatic attraction and surface complexation dominated by chemisorption likely accounted for the enhanced sorptive interactions between zeolites and organic compounds. Similarly, the adsorption capacity of the treated MK toward Cu(II) and Pb(II) increased almost 20-fold, which

was 431.0 mg g^{-1} for Cu(II) and 337.8 mg g^{-1} for Pb(II). The ionic exchange reaction between the heavy metal ions and enriched sodium ion resulted in heavy metal removal by the MK-based zeolites. Therefore, the hydrothermally synthesized MK-based zeolites may be used as sorbents for wastewater treatment to remove organic pollutants and heavy metals with no significant toxicity risk.

Acknowledgements

We thank the financial support from Zhejiang University of Technology (No. 2017129004429). We also thank Dr. Bin Cao for contributing several chemicals and for helpful discussion.

References

[1] S.B. Wang, Y.L. Peng, Natural zeolites as effective adsorbents in water and wastewater treatment, Chem. Eng. J. 156 (2010) 11-24.

[2] E. Erdem, N. Karapinar, R. Donat, The removal of heavy metal cations by natural zeolites, J. Colloid Interf. Sci. 280 (2004) 309-314.

[3] H. Liu, S. Peng, L. Shu, T. Chen, T. Bao, R.L. Frost, Magnetic zeolite NaA: synthesis, characterization based on metakaolin and its application for the removal of Cu^{2+}, Pb^{2+}, Chemosphere, 91 (2013) 1539-1546.

[4] B. Ersoy, M.S. Celik, Uptake of aniline and nitrobenzene from aqueous solution by organo-zeolite, Environ. Technol. 25 (2004) 341-348.

[5] J. Lemic, D. Kovacevic, M. Tomasevic-Canovic, D. Kovacevic, T. Stanic, R. Pfend,

395 Removal of atrazine, lindane and diazinone from water by organo-zeolites, Water Res. 40
396 (2006) 1079-1085.
397 [6] Z.H. Li, T. Burt, R.S. Bowman, Sorption of ionizable organic solutes by surfactant modified
398 zeolite, Environ. Sci. Technol. 34 (2000) 3756-3760.
399 [7] C. Li, Y. Dong, D. Wu, L. Peng, H. Kong, Surfactant modified zeolite as adsorbent for
400 removal of humic acid from water, Appl. Clay Sci. 52 (2011) 353-357.
401 [8] J. Xie, W. Meng, D. Wu, Z. Zhang, H. Kong, Removal of organic pollutants by surfactant
402 modified zeolite: comparison between ionizable phenolic compounds and non-ionizable
403 organic compounds, J. Hazard. Mater. 231-232 (2012) 57-63.
404 [9] M.A. Grace, M.G. Healy, E. Clifford, Use of industrial by-products and natural media to
405 adsorb nutrients, metals and organic carbon from drinking water, Sci. Total Environ. 518-
406 519 (2015) 491-497.
407 [10] M. Alkan, Ç. Hopa, Z. Yilmaz, H. Güler, The effect of alkali concentration and solid/liquid
408 ratio on the hydrothermal synthesis of zeolite NaA from natural kaolinite, Micropor.
409 Mesopor. Mat. 86 (2005) 176-184.
410 [11] H. Youssef, D. Ibrahim, S. Komarneni, Microwave-assisted versus conventional synthesis
411 of zeolite A from metakaolinite, Micropor. Mesopor. Mat. 115 (2008) 527-534.
412 [12] S. Chandrasekhar, P.N. Pramada, Microwave assisted synthesis of zeolite A from
413 metakaolin, Micropor. Mesopor. Mat. 108 (2008) 152-161.
414 [13] C.S. Cundy, P.A. Cox, The hydrothermal synthesis of zeolites: Precursors, intermediates
415 and reaction mechanism, Micropor. Mesopor. Mat. 82 (2005) 1-78.
416 [14] C.A. Rios Reyes, C.D. Williams, O.M. Castellanos Alarcon, Synthesis of zeolite LTA from

417 thermally treated kaolinite, Rev. Fac. Ing. Univ. Antioquia 53 (2010) 30-41.
418 [15] C.A. Rios, C.D. Williams, M.A. Fullen, Hydrothermal synthesis of hydrogarnet and
419 tobermorite at 175 °C from kaolinite and metakaolinite in the $CaO-Al_2O_3-SiO_2-H_2O$
420 system: A comparative study, Appl. Clay Sci. 43 (2009) 228-237.
421 [16] C.A. Rios, C.D. Williams, M.A. Fullen, Nucleation and growth history of zeolite LTA
422 synthesized from kaolinite by two different methods, Appl. Clay Sci. 42 (2009) 446-454.
423 [17] H.W. Luo, Y.C. Wu, A.Q. Zhao, A. Kumar, Y.Q. Liu, B. Cao, E.H. Yang, Hydrothermally
424 synthesized porous materials from municipal solid waste incineration bottom ash and their
425 interfacial interactions with chloroaromatic compounds, J. Clean. Prod. 162 (2017) 411-
426 419.
427 [18] H.W. Luo, L.F. Wang, Z.H. Tong, H.Q. Yu, G.P. Sheng, Approaching the binding between
428 Cu(II) and aerobic granules by a modified titration and μ-XRF, Front. Env. Sci. Eng. 10
429 (2016) 362-367.
430 [19] H.W. Luo, J.J. Chen, G.P. Sheng, J.H. Su, S.Q. Wei, H.Q. Yu, Experimental and theoretical
431 approaches for the surface interaction between copper and activated sludge
432 microorganisms at molecular scale, Sci. Rep. 4 (2014) 7078.
433 [20] Y.B. Wang, L. Huang, R. Lau, Conversion of municipal solid waste incineration bottom
434 ash to sorbent material for pollutants removal from water, J. Taiwan Inst. Chem. E. 60
435 (2016) 275-286.
436 [21] G. Kakali, T. Perraki, S. Tsivilis, E. Badogiannis, Thermal treatment of kaolin: the effect
437 of mineralogy on the pozzolanic activity, Appl. Clay Sci. 20 (2001) 73-80.
438 [22] M. Bellotto, A. Gualtieri, G. Artioli, S.M. Clark, Kinetic study of the kaolinite-mullite

439 reaction sequence. Part I: Kaolinite dehydroxylation, Phys. Chem. Miner. 22 (1995) 207-
440 214.
441 [23] M. Gougazeh, J.C. Buhl, Synthesis and characterization of zeolite A by hydrothermal
442 transformation of natural Jordanian kaolin, J. Assoc. Arab Univ. Basic Appl. Sci. 15 (2014)
443 35-42.
444 [24] L. Heller-Kallai, I. Lapides, Reactions of kaolinites and metakaolinites with NaOH-
445 comparison of different samples (Part 1), Appl. Clay Sci. 35 (2007) 99-107.
446 [25] W. Kim, D. Choi, S. Kim, Sonochemical synthesis of zeolite A from metakaolinite in
447 NaOH solution, Mater. Trans. 51 (2010) 1694-1698.
448 [26] A. Demortier, N. Gobeltz, J.P. Lelieur, C. Duhayon, Infrared evidence for the formation
449 of an intermediate compound during the synthesis of zeolite Na-A from metakaolin, Int.
450 J. Inorg. Mater. 1 (1999) 129-134.
451 [27] I. Hassan, S.M. Antao, J.B. Parise, Cancrinite: Crystal structure, phase transitions, and
452 dehydration behavior with temperature, Am. Mineral. 91 (2006) 1117-1124.
453 [28] E.M. Flanigen, H. Khatami, H.A. Szymanski, Infrared Structural Studies of Zeolite
454 Frameworks. In: Flanigen, E.M. and Sand, L.B., Ed., Molecular Sieve Zeolites, Advances
455 in Chemistry 101, American Chemical Society, Washington DC, (1971) 201-229.
456 [29] B.B. Kenne Diffo, A. Elimbi, M. Cyr, J. Dika Manga, H. Tchakoute Kouamo, Effect of
457 the rate of calcination of kaolin on the properties of metakaolin-based geopolymers, J.
458 Asian Ceram. Soc. 3 (2015) 130-138.
459 [30] B. Lothenbach, K. Scrivener, R.D. Hooton, Supplementary cementitious materials, Cem.
460 Concr. Res. 41 (2011) 1244-1256.

461 [31] M.M.J. Treacy, J.B. Higgins, Collections of Simulated XRD Powder Patterns for Zeolites,
462 4th Ed. Elsevier, Amsterdam, The Netherlands, (2001) 1-586.
463 [32] H. Zhao, Y. Deng, J.B. Harsh, M. Flury, J.S. Boyle, Alteration of kaolinite to cancrinite
464 and sodalite by simulated hanford tank waste and its impact on cesium retention, Clays
465 Clay Miner. 52 (2004) 1-13.
466 [33] R. Grizzetti, G. Artioli, Kinetics of nucleation and growth of zeolite LTA from clear
467 solution by in situ and ex situ XRPD, Micropor. Mesopor. Mat. 54 (2002) 105-112.
468 [34] D. Sabatino, B.D. Sabatino, D. Gimeno, C. Pace, Synthesis and characterization of Na-X,
469 Na-A and Na-P zeolites and hydroxysodalite from metakaolinite, Clay Miner. 46 (2011)
470 339-354.
471 [35] X.Y. Ke, S.A. Bernal, N. Ye, J.L. Provis, J.K. Yang, One-part geopolymers based on
472 thermally treated red mud/NaOH blends, J. Am. Ceram. Soc. 98 (2015) 5-11.
473 [36] Y.W. Chiang, R.M. Santos, K. Vanduyfhuys, B. Meesschaert, J.A. Martens, Atom-efficient
474 route for converting incineration ashes into heavy metal sorbents, Chem. Sus. Chem. 7
475 (2014) 276-283.
476 [37] M. Thommes, K. Kaneko, A.V. Neimark, J.P. Olivier, F. Rodriguez-Reinoso, J. Rouquerol,
477 K.S.W. Sing, Physisorption of gases, with special reference to the evaluation of surface
478 area and pore size distribution (IUPAC Technical Report), Pure Appl. Chem. 87 (2015)
479 1051-1069.
480 [38] S. Angioi, S. Polati, M. Roz, C. Rinaudo, V. Gianotti, M.C. Gennaro, Sorption studies of
481 chloroanilines on kaolinite and montmorillonite, Environ. Pollut. 134 (2005) 35-43.
482 [39] L. Zuo, W. Song, T. Shi, C. Lv, J. Yao, J. Liu, Y. Weng, Adsorption of aniline on template-

483 synthesized porous carbons, Micropor. Mesopor. Mat. 200 (2014) 174-181.
484 [40] D.-W. Gao, Q. Hu, H. Pan, J. Jiang, P. Wang, High-capacity adsorption of aniline using
485 surface modification of lignocellulose-biomass jute fibers, Bioresource Technol. 193
486 (2015) 507-512.
487 [41] M. Salman, B. El-Eswed, F. Khalili, Adsorption of humic acid on bentonite, Appl. Clay
488 Sci. 38 (2007) 51-56.
489 [42] M.S., Rahman, M.R., Islam, Effects of pH on Isotherms Modeling for Cu(II) Ions
490 Adsorption Using Maple Wood Sawdust. Chem. Eng. J. 149 (2009) 273-280
491 [43] Q. Fan, Z. Li, H. Zhao, Z. Jia, J. Xu, W. Wu, Adsorption of Pb(II) on palygorskite from
492 aqueous solution: Effects of pH, ionic strength and temperature, Appl. Clay Sci. 45 (2009)
493 111-116
494 [44] U. Wingenfelder, C. Hansen, G. Furrer, R. Schulin, Removal of heavy metals from mine
495 waters by natural zeolites, Environ. Sci. Technol. 39 (2005) 4606-4613.
496 [45] S. Andrejkovičová, A. Sudagar, J. Rocha, C. Patinha, W. Hajjaji, E.F. da Silva, A. Velosa,
497 F. Rocha, The effect of natural zeolite on microstructure, mechanical and heavy metals
498 adsorption properties of metakaolin based geopolymers, Appl. Clay Sci. 126 (2016) 141-
499 152.
500 [46] T.W. Cheng, M.L. Lee, M.S. Ko, T.H. Ueng, S.F. Yang, The heavy metal adsorption
501 characteristics on metakaolin-based geopolymer, Appl. Clay Sci. 56 (2012) 90-96.

Table 1. Chemical compositions of the raw and treated metakaolin

Component	Content (wt.%)	
	Raw MK	Treated MK
SiO_2	53.01	41.32
Al_2O_3	43.74	34.36
TiO_2	1.70	1.18
Fe_2O_3	0.43	0.35
Na_2O	0.23	21.79
K_2O	0.19	0.14
MgO	0.03	0.02
P_2O_5	0.03	0.02
SO_3	0.03	0.01
CaO	0.02	0.01
Total	99.41	99.20

Figure Captions

Fig. 1 SEM micrographs of the raw (upper) and hydrothermally treated (bottom) metakaolin.

Fig. 2 (a) FT-IR spectra, (b) XRD diffractograms, and (c) TGA curves of the raw (black line) and the hydrothermally treated (red line) metakaolin.

Fig. 3 (a) N_2 adsorption-desorption isotherms at -196 °C, (b) cumulative pore volume, and (c) desorption BJH pore size distribution of the raw (black line) and the hydrothermally treated (red line) metakaolin.

Fig. 4 Time-dependent adsorption of organic pollutants: (a) AN and 3-CA, and (b) humic acid by the raw and the hydrothermally treated metakaolin at pH 7.2. Error bars represent one standard deviation of triplicate samples.

Fig. 5 Time-dependent adsorption of heavy metals: (a) Cu(II) at pH 3.0 and 5.0, and (b) Pb(II) at pH 5.0 by the raw and the hydrothermally treated metakaolin. Error bars represent one standard deviation of triplicate samples.

Fig. 6 Linearized Langmuir adsorption isotherms of (a) Cu(II) and (b) Pb(II) on the raw metakaolin, and (c) Cu(II) and (d) Pb(II) on the hydrothermally treated metakaolin at pH 5.0. Error bars represent one standard deviation of triplicate samples.

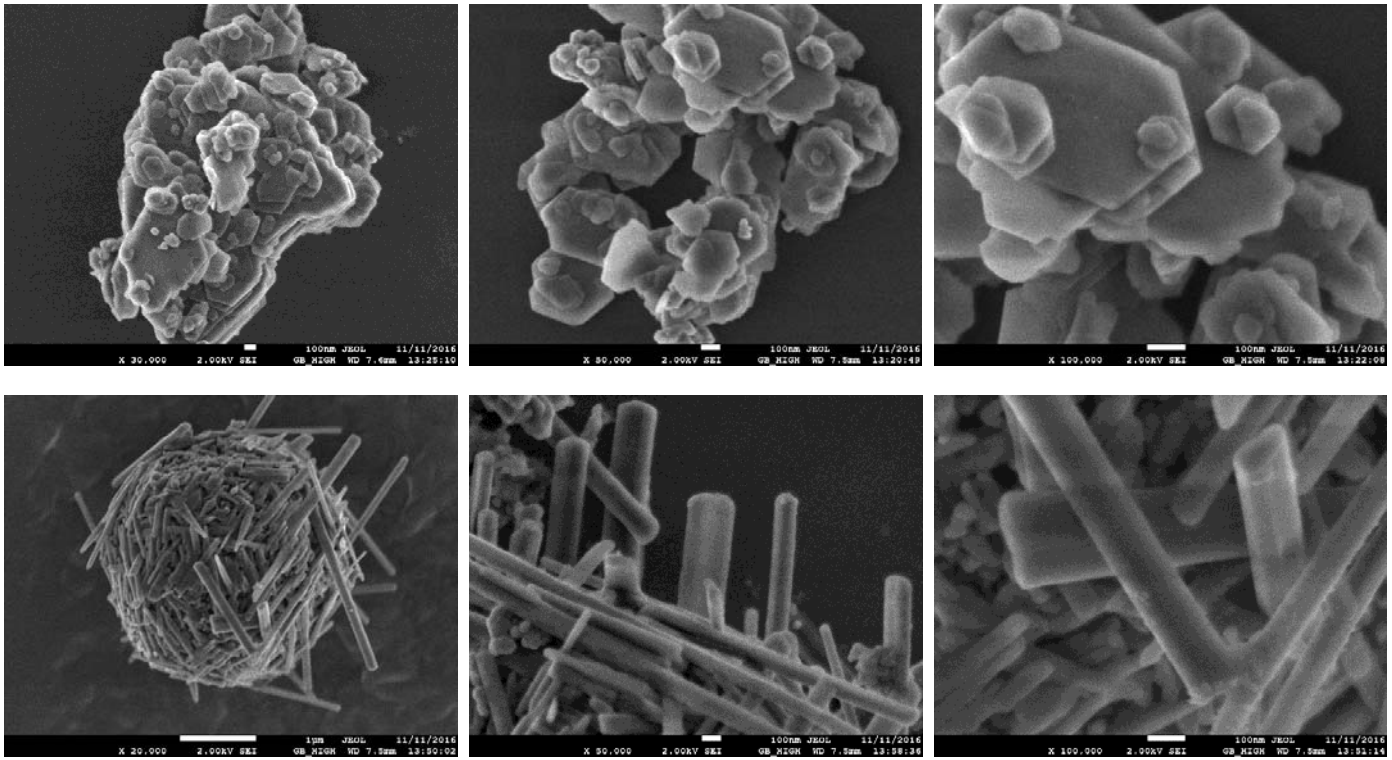
X 30,000 2.00kV SEI 100nm JEOL 11/11/2016 GB_HIGH WD 7.4mm 13:25:10
X 50,000 2.00kV SEI 100nm JEOL 11/11/2016 GB_HIGH WD 7.5mm 13:20:49
X 100,000 2.00kV SEI 100nm JEOL 11/11/2016 GB_HIGH WD 7.5mm 13:22:08
X 20,000 2.00kV SEI 1μm JEOL 11/11/2016 GB_HIGH WD 7.5mm 13:50:02
X 50,000 2.00kV SEI 100nm JEOL 11/11/2016 GB_HIGH WD 7.5mm 13:58:36
X 100,000 2.00kV SEI 100nm JEOL 11/11/2016 GB_HIGH WD 7.5mm 13:51:14

Fig. 1

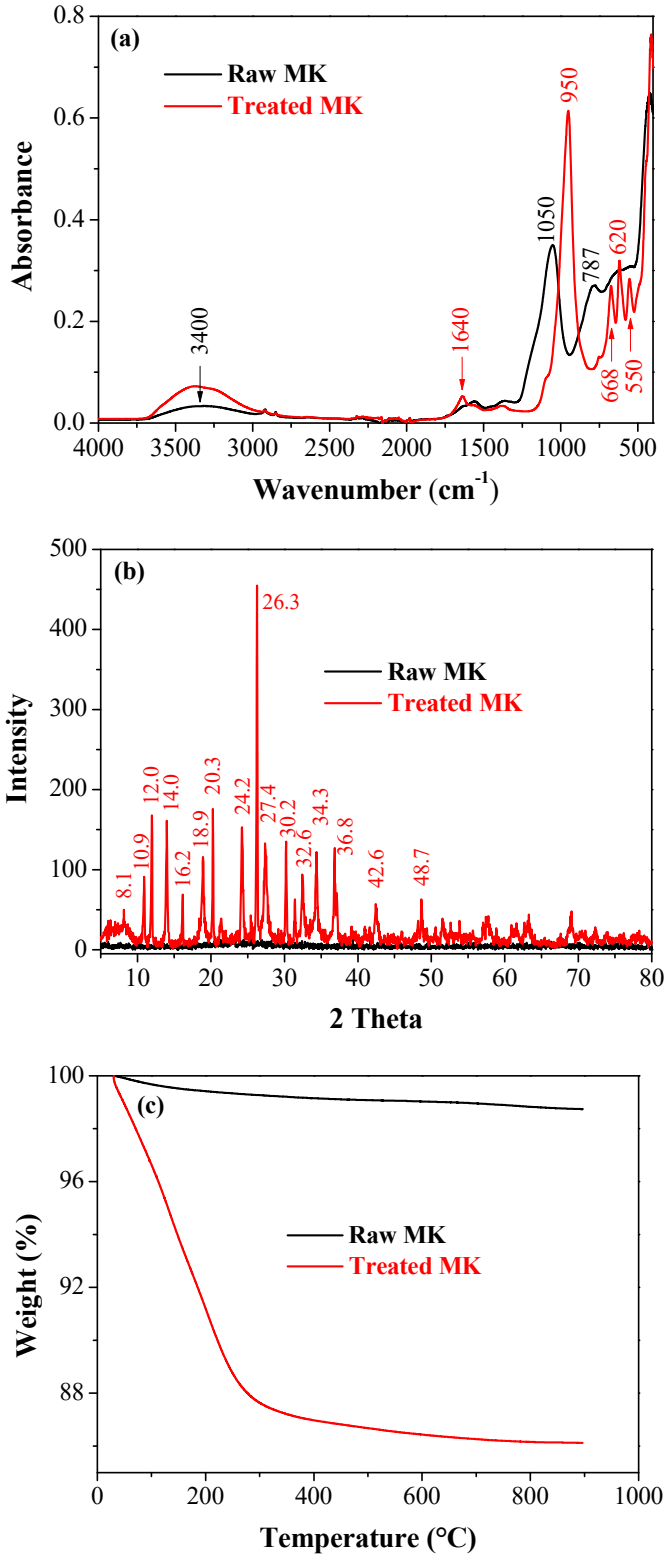
(a)
Raw MK
Treated MK
Absorbance
Wavenumber (cm-1)
3400
1640
1050
950
787
620
668
550
(b)
Raw MK
Treated MK
Intensity
2 Theta
26.3
12.0
14.0
20.3
24.2
27.4
30.2
34.3
36.8
10.9
16.2
18.9
32.6
42.6
48.7
8.1
(c)
Raw MK
Treated MK
Weight (%)
Temperature (°C)

Fig. 2

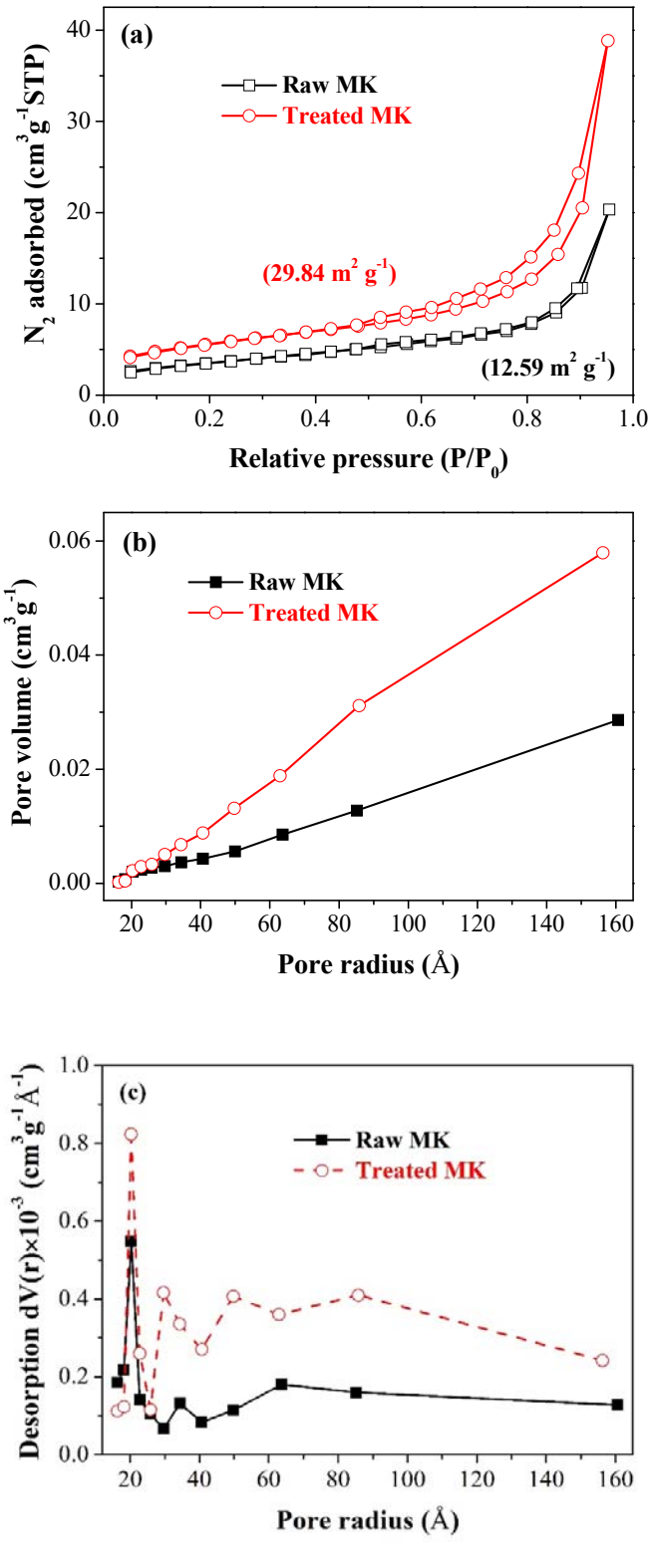
(a)
Raw MK
Treated MK
(29.84 m² g⁻¹)
(12.59 m² g⁻¹)
N₂ adsorbed (cm³ g⁻¹STP)
Relative pressure (P/P₀)
(b)
Raw MK
Treated MK
Pore volume (cm³ g⁻¹)
Pore radius (Å)
(c)
Raw MK
Treated MK
Desorption dV(r)×10⁻³ (cm³ g⁻¹ Å⁻¹)
Pore radius (Å)

Fig. 3

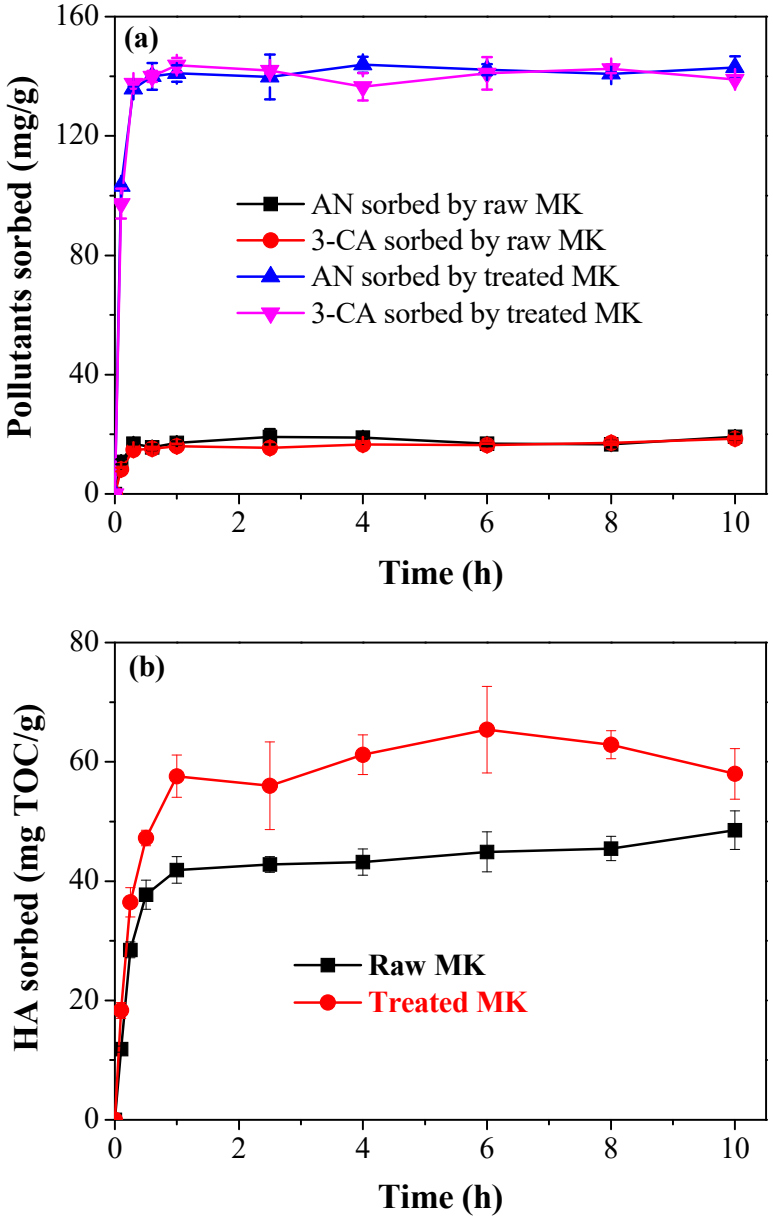
(a)
Pollutants sorbed (mg/g)
Time (h)
AN sorbed by raw MK
3-CA sorbed by raw MK
AN sorbed by treated MK
3-CA sorbed by treated MK
(b)
HA sorbed (mg TOC/g)
Time (h)
Raw MK
Treated MK

Fig. 4

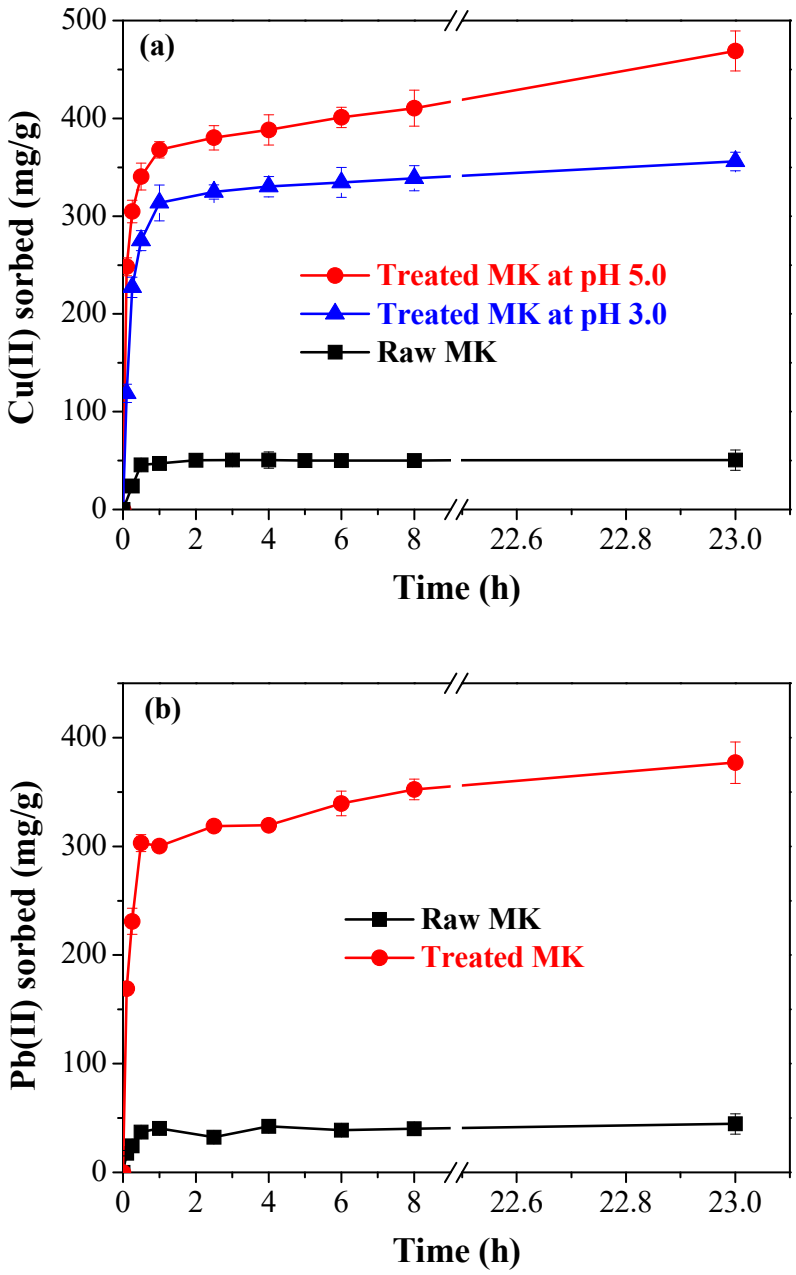
(a)
Cu(II) sorbed (mg/g)
Time (h)
Treated MK at pH 5.0
Treated MK at pH 3.0
Raw MK
(b)
Pb(II) sorbed (mg/g)
Time (h)
Raw MK
Treated MK

Fig. 5

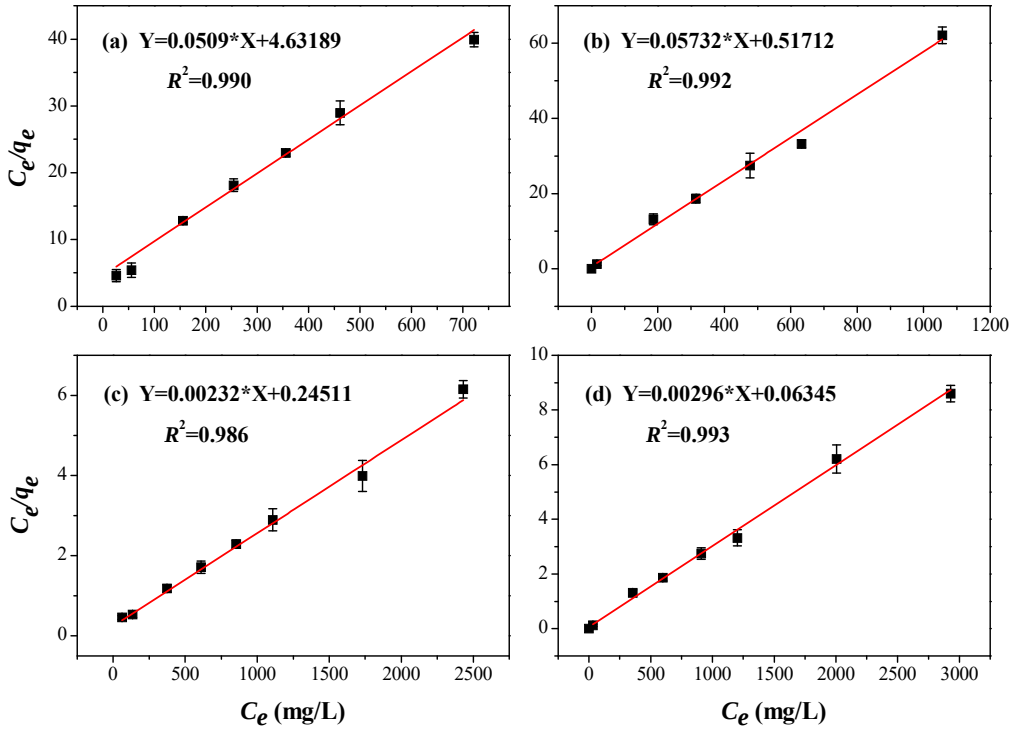
(a) Y=0.0509*X+4.63189
R^2=0.990
(b) Y=0.05732*X+0.51712
R^2=0.992
(c) Y=0.00232*X+0.24511
R^2=0.986
(d) Y=0.00296*X+0.06345
R^2=0.993
C_e/q_e
C_e (mg/L)

Fig. 6